AGU PUBLICATIONS

JGR

Journal of Geophysical Research: Atmospheres

RESEARCH ARTICLE
10.1002/2013JD021290

Key Points:
- Broad spatial patterns of 24 h average nitrate are simulated well
- Underprediction of sodium limits partitioning of nitrate to particles in LA
- Nocturnal nitrate production is impacted by modeling of evening PBL transition

Supporting Information:
- Tables S1–S11 and Figures S1–S48

Correspondence to:
J. T. Kelly,
kelly.james@epa.gov

Citation:
Kelly, J. T., et al. (2014), Fine-scale simulation of ammonium and nitrate over the South Coast Air Basin and San Joaquin Valley of California during CalNex-2010, *J. Geophys. Res. Atmos.*, *119*, 3600–3614, doi:10.1002/2013JD021290.

Received 1 DEC 2013
Accepted 27 FEB 2014
Accepted article online 3 MAR 2014
Published online 28 MAR 2014

Fine-scale simulation of ammonium and nitrate over the South Coast Air Basin and San Joaquin Valley of California during CalNex-2010

James T. Kelly[1], Kirk R. Baker[1], John B. Nowak[2,3], Jennifer G. Murphy[4], Milos Z. Markovic[4,5], Trevor C. VandenBoer[4,6], Raluca A. Ellis[4,7], J. Andrew Neuman[2,3], Rodney J. Weber[8], James M. Roberts[3], Patrick R. Veres[2,3], Joost A. de Gouw[2,3], Melinda R. Beaver[9,10], Sally Newman[11], and Chris Misenis[1]

[1]Office of Air Quality Planning and Standards, U.S. EPA, Research Triangle Park, North Carolina, USA, [2]Cooperative Institute for Research in Environmental Sciences, University of Colorado Boulder, Boulder, Colorado, USA, [3]Chemical Sciences Division, Earth System Research Laboratory, NOAA, Boulder, Colorado, USA, [4]Department of Chemistry, University of Toronto, Toronto, Ontario, Canada, [5]Now at NOAA and University of Colorado, Boulder, Colorado, USA, [6]Now at Department of Chemistry, Memorial University of Newfoundland, St. John's, Newfoundland and Labrador, Canada, [7]Now at Climate and Urban Systems Partnership, Franklin Institute, Philadelphia, Pennsylvania, USA, [8]School of Earth and Atmospheric Sciences, Georgia Institute of Technology, Atlanta, Georgia, USA, [9]Environmental Science and Engineering, California Institute of Technology, Pasadena, California, USA, [10]Now at National Exposure Research Laboratory, U. S. EPA, Research Triangle Park, North Carolina, USA, [11]Division of Geological and Planetary Sciences, California Institute of Technology, Pasadena, California, USA

Abstract National ambient air quality standards (NAAQS) have been set for $PM_{2.5}$ due to its association with adverse health effects. $PM_{2.5}$ design values in the South Coast Air Basin (SoCAB) and San Joaquin Valley of California exceed NAAQS levels, and NH_4^+ and NO_3^- make up the largest fraction of total $PM_{2.5}$ mass on polluted days. Here we evaluate fine-scale simulations of $PM_{2.5}$ NH_4^+ and NO_3^- with the Community Multiscale Air Quality model using measurements from routine networks and the California Research at the Nexus of Air Quality and Climate Change 2010 campaign. The model correctly simulates broad spatial patterns of NH_4^+ and NO_3^- including the elevated concentrations in eastern SoCAB. However, areas for model improvement have been identified. NH_3 emissions from livestock and dairy facilities appear to be too low, while those related to waste disposal in western SoCAB may be too high. Analyses using measurements from flights over SoCAB suggest that problems with NH_3 predictions can influence NO_3^- predictions there. Offline ISORROPIA II calculations suggest that overpredictions of NH_x in Pasadena cause excessive partitioning of total nitrate to the particle phase overnight, while underpredictions of Na^+ cause too much partitioning to the gas phase during the day. Also, the model seems to underestimate mixing during the evening boundary layer transition leading to excessive nitrate formation on some nights. Overall, the analyses demonstrate fine-scale variations in model performance within and across the air basins. Improvements in inventories and spatial allocations of NH_3 emissions and in parameterizations of sea spray emissions, evening mixing processes, and heterogeneous $ClNO_2$ chemistry could improve model performance.

1. Introduction

U.S. Environmental Protection Agency's (U.S. EPA) integrated science assessment determined that $PM_{2.5}$ (particulate matter with aerodynamic diameter < 2.5 μm) exposure has a causal or "likely to be causal" relationship with adverse health outcomes including mortality as well as with negative welfare effects [*U.S. Environmental Protection Agency* (*U.S. EPA*), 2009]. Accordingly, the national ambient air quality standards (NAAQS) for $PM_{2.5}$ are currently set at 12 μg m^{-3} on an annual basis and 35 μg m^{-3} on a 24 h basis to protect human health. Despite much progress in recent decades [*South Coast Air Quality Management District* (*SCAQMD*), 2013; *San Joaquin Valley Air Pollution Control District (SJVAPCD)*, 2012], $PM_{2.5}$ design values (DVs) at monitors in the South Coast Air Basin (SoCAB) and San Joaquin Valley (SJV) of California remain well above the NAAQS levels. Note that a DV is a statistic that describes the air quality status of a given location relative to the level of the NAAQS. The highest 2010–2012 annual $PM_{2.5}$ DV is 19 μg m^{-3} in SJV and 15.6 μg m^{-3} in SoCAB, while the highest 24 h $PM_{2.5}$ DV is 59 μg m^{-3} in SJV and 37 μg m^{-3} in SoCAB [*U.S. EPA*, 2013]. At key monitors in SJV and SoCAB, ammonium (NH_4^+) and nitrate (NO_3^-) made up more than 50% of total $PM_{2.5}$ mass on highly polluted days in recent years [*SCAQMD*, 2013; *SJVAPCD*, 2012].

Photochemical models are often used to understand the processes that lead to elevated NH_4^+ and NO_3^- concentrations in SoCAB and SJV and the potential response of these pollutants to precursor emission reduction. Modeling studies have indicated that NO_x emission reductions are effective for reducing NH_4^+ and NO_3^- concentrations in these areas [e.g., *SCAQMD*, 2013; *SJVAPCD*, 2012; *Kleeman et al.*, 2005], and NO_x emissions reductions are also considered desirable due to associated reductions in ozone during summer months [*Pusede and Cohen,* 2012; *SCAQMD*, 2013]. Some secondary organic aerosol (SOA) constituents such as organic nitrates observed in California could also decrease with decreasing NO_x emissions [*Rollins et al.*, 2012], although the overall impact of NO_x emission reductions on SOA levels is an area of active research [e.g., *Pye et al.*, 2013]. While reductions in NH_4^+ and NO_3^- following previous NO_x emissions reductions point to the success of photochemical modeling for air quality management in California, simulating NH_4^+ and NO_3^- in SoCAB and SJV remains challenging due to the complex meteorology, emissions, and terrain in these regions.

Since SoCAB is often close to the center of the Pacific high-pressure system, SoCAB meteorology is frequently influenced by large-scale subsidence inversions that limit vertical ventilation of the basin, while mountain ranges limit horizontal ventilation. SoCAB is also impacted by local-scale meteorology including upslope-downslope mountain flows and land-sea breezes that transport air from the LA urban core into the eastern basin during the day with weaker return flows overnight [*Jacobson*, 2002; *Lu and Turco*, 1996]. The complex SoCAB flows transport diverse emissions including those from the western ports of LA and Long Beach, heavy-duty diesel vehicle activity associated with goods movement and the ports [*Bishop et al.*, 2012], light-duty vehicle [*Bishop et al.*, 2010], and other activity that supports a population of more than 15 million, and numerous dairy facilities in the eastern basin. Elevated NH_4^+ and NO_3^- concentrations occur in eastern SoCAB when NH_3 emissions from dairy facilities are injected into air masses with aged NO_x emissions from the LA urban core [*Russell and Cass*, 1986]. Multiday pollution episodes can also occur when pollutants from the previous nighttime residual layer are mixed to the surface in morning or when aged pollution in the Santa Monica Bay is reintroduced into SoCAB [*Riedel et al.*, 2012; *Young et al.*, 2012; *Lu and Turco*, 1996].

Air pollution processes in SJV are also driven by complex interactions between meteorology, emissions, and terrain. Severe wintertime $PM_{2.5}$ episodes with high NH_4^+ and NO_3^- concentration develop in the valley under cool, stagnant, and humid conditions where air is constrained by mountain ranges in the horizontal and temperature (*T*) inversions in the vertical. Conceptual models of these episodes involve the trapping of primary $PM_{2.5}$ emissions overnight in a shallow surface layer below a radiation inversion and the mixing of NH_3 from daytime emissions in rural areas with NO_x from urban areas in a valley-wide layer above the radiation inversion and below a persistent subsidence inversion aloft. The NH_4^+ and NO_3^- that forms aloft overnight are then mixed to the surface in the morning when the radiation inversion breaks [*Herner et al.*, 2006]. In addition to having meteorology conducive to NH_4^+ and NO_3^- formation, SJV is impacted by diverse emissions associated with its population of about 4 million that is projected to increase substantially in coming decades [*California Department of Finance*, 2013; *Hixson et al.*, 2012]. Also, large emissions of NH_3 occur in SJV as a by-product of its agricultural sector. Seven of the top 10 agricultural counties in California's massive agricultural industry ($43.5 billion in 2011) are located in SJV, with Tulare, Fresno, and Kern Counties ranking as the top 3 counties in California in terms of livestock (cattle and calf) population [*California Department of Food and Agriculture*, 2013]. SJV is also a major corridor for goods movement and experiences substantial NO_x emissions from heavy-duty diesel trucks that move goods between Mexico and Canada on I-5 and between major SJV cities on Highway 99. Although peak $PM_{2.5}$ episodes occur in wintertime in SJV, this area is in nonattainment of the annual $PM_{2.5}$ NAAQS and nonnegligible concentrations NH_4^+ and NO_3^- exist in all seasons.

Typical NH_4^+ and NO_3^- modeling assessments include a model performance evaluation where predictions are evaluated against data from routine monitoring networks such as U.S. EPA's Chemical Speciation Network (CSN) [e.g., *Simon et al.*, 2012]. While these evaluations can demonstrate a model's ability to predict NH_4^+ and NO_3^- concentrations, they are generally of limited diagnostic value since CSN measurements have low time resolution (24 h), observations of precursor gases (i.e., NH_3 and HNO_3) and key meteorological variables are mostly unavailable, and network observations have limited spatial coverage. Thorough diagnostic evaluations can be performed using comprehensive data sets from intensive field campaigns to develop air quality models and provide additional support for their use in decision making. These evaluations are especially important for fine-scale simulations of

secondary pollutants such as NH_4^+ and NO_3^- in complex environments such as SoCAB and SJV that resolve detailed air pollution processes under challenging conditions. Fine-scale modeling (i.e., 4 km horizontal resolution) is currently used for air quality management in California [*SCAQMD*, 2013; *SJVAPCD*, 2012] and in research studies focused on California [e.g., *Angevine et al.*, 2012; *Baker et al.*, 2013; *Ensberg et al.*, 2013; *Fast et al.*, 2012; *Kelly et al.*, 2011; *Ying,* 2011], while national-scale assessments use coarser resolution (generally 12 to 50 km) for computational efficiency [*Schifer et al.*, 2014; *Huang et al.*, 2013; *U.S. EPA*, 2012a; *Walker et al.*, 2012; *Heald et al.*, 2012].

In May–July 2010, the California Research at the Nexus of Air Quality and Climate Change (CalNex-2010) study was conducted to address issues related to air quality and climate change [*Ryerson et al.*, 2013]. The vast CalNex-2010 data set includes airborne and ground measurements of NH_3, HNO_3, NO_3^-, and NH_4^+ at hourly and subhourly time resolutions along with many complementary chemical and meteorology measurements in SoCAB and SJV. Here we evaluate the ability of a fine-scale photochemical model simulation to predict observed concentrations of $PM_{2.5}$ NO_3^- and NH_4^+ at surface sites as well as NH_3 and HNO_3 along aircraft flight paths and at surface sites. Additionally, we evaluate predictions of many complementary chemical species and meteorological variables and conduct offline thermodynamic modeling to interpret gas-particle partitioning results.

2. Methods

Air quality was simulated over California from 4 May to 30 June 2010 with the Community Multiscale Air Quality (CMAQ) model version 5.0.1 (http://cmascenter.org/cmaq/). The model grid covered nearly all of California and Nevada as well as parts of the Pacific Ocean, Mexico, and Arizona with 4 km horizontal resolution and 34 vertical layers (see Figure S1 in the supporting information for model domain). Inorganic aerosol thermodynamics was simulated within CMAQ's modal aerosol formulations using ISORROPIA II [*Fountoukis and Nenes*, 2007], gas-phase chemistry was simulated with the Carbon Bond 05 chemical mechanism [*Yarwood et al.*, 2005], and heterogeneous hydrolysis of N_2O_5 was treated according to *Davis et al.* [2008]. Chemical boundary conditions (3-hourly) were derived from a GEOS-Chem v8-03-02 global model simulation (http://acmg.seas.harvard.edu/geos/). The prognostic meteorological fields used to drive CMAQ were based on a simulation with the Weather Research and Forecasting (WRF; www.wrf-model.org) model version 3.4 using a grid consistent with that of CMAQ. WRFv3.4 was configured with the asymmetric convective model version 2 planetary boundary layer (PBL) scheme [*Pleim*, 2007] and the Pleim-Xiu land surface model [*Pleim and Xiu*, 2003]. A meteorological simulation for the same period and configuration used here but based on an earlier version of WRF (version 3.1) has been evaluated in detail previously [*Baker et al.*, 2013].

Point source emissions for the modeling period were based on state-submitted 2010 emission totals and day-specific continuous emissions monitor data when available. Other anthropogenic, nonmobile source emissions were based on the 2008 National Emissions Inventory (NEI08) version 2 as processed using the Sparse Matrix Operator Kernel Emissions (SMOKE) model (http://www.cmascenter.org/smoke/). Mobile source emission totals were based on 2007 and 2011 emission totals provided by the California Air Resources Board (CARB) that were interpolated to 2010. Spatial and temporal allocations of mobile source emissions were based on SMOKE-MOVES (Motor Vehicle Emissions Simulator, http://www.epa.gov/otaq/models/moves) simulations. The scaling approach for combining CARB emission totals with SMOKE-MOVES allocations is described elsewhere [*U.S. EPA*, 2012b]. Biogenic emissions are estimated using the biogenic emissions inventory system version 3.14 with hour-specific T and solar radiation based on WRF output.

Information on the surface observation sites considered here is provided in Table S1, and site locations are illustrated in Figure S1 in the supporting information. Measurements of 24 h average inorganic $PM_{2.5}$ concentration at the CSN sites were acquired from the CARB 2012 Air Quality Data DVD (www.arb.ca.gov/aqd/aqdcd/aqdcd.htm). Measurements from the CalNex-2010 study were obtained through online data resources for the Pasadena site (www.esrl.noaa.gov/csd/tropchem/2010calnex/Ground/DataDownload), the Bakersfield site (https://bspace.berkeley.edu/portal/), and the NOAA WP-3 aircraft (www.esrl.noaa.gov/csd/tropchem/2010calnex/P3/DataDownload). Summary information on the relevant CalNex-2010 measurements is provided in Table 1 along with references to primary publications. Additional CalNex-2010 measurements used in the supporting information are described there.

Table 1. CalNex-2010 Measurements Used Here

Location	Measurement	Reference	Technique	Sample Interval
Pasadena	NH_3	*Ellis et al.* [2010]	Quantum cascade tunable infrared laser differential absorption spectroscopy	1 h
Pasadena	HCl and HNO_3	*Veres et al.* [2008]	Negative ion proton transfer chemical ionization mass spectrometry (CIMS)	1 min[a]
Pasadena	NO_3^-, SO_4^{2-}, NH_4^+, Cl^-, Na^+, and K^+	*Weber et al.* [2001]	Particle into liquid sampling and ion chromatography (IC)	10 min[a]
Pasadena	PBL height	*Haman et al.* [2012]	Vaisala Ceilometer CL31	
Pasadena	*T*, RH, wind speed, and wind direction		Davis VantagePro2 weather station on Caltech Millikan Library	
Bakersfield	NO_3^-, SO_4^{2-}, NH_4^+, Cl^-, NH_3, SO_2, and HCl	*Markovic et al.* [2012]	Ambient Ion Monitor-IC	1 h
Bakersfield	HNO_3	*Crounse et al.* [2006]	CIMS	0.5 s[a]
NOAA WP-3	NH_3	*Nowak et al.* [2007]	Protonated acetone dimer CIMS	1 s[b]
NOAA WP-3	HNO_3	*Neuman et al.* [2002]	SiF_5^- CIMS	1 s[b]

[a]Averaged to 1 h for comparison with CMAQ hourly average concentration predictions.
[b]CMAQ instantaneous mixing ratios at each hour were interpolated in time to match 1 s aircraft measurements.

3. Results and Discussion

3.1. Evaluation Using CSN Observations

Predictions of 24 h average concentrations of inorganic $PM_{2.5}$ components were evaluated against observations at CSN sites in SoCAB and SJV. Time series of modeled and observed NO_3^- concentrations at the sites are shown in Figure 1. Time series for NH_4^+, SO_4^{2-}, Ca^{2+}, Mg^{2+}, Na^+, and K^+ are provided in Figures S2–S5, and a statistical comparison is provided in Table S3 for the metrics used in this study: normalized mean bias (NMB), normalized mean error (NME), root-mean-square error, and Pearson correlation coefficient (*r*).

The Riverside-Rubidoux monitor (Rvrside-Rubi) experienced the highest NO_3^- concentrations of the CSN sites with an observed mean ± standard deviation of 6.81 ± 3.47 μg m^{-3} (Figure 1c). Good correlation ($r = 0.78$) exists between model predictions and observations of NO_3^- at this monitor suggesting that the model generally captures the processes leading to NO_3^- formation. However, predictions are biased low during the period of elevated observed concentrations in June and the overall NMB is −39.8%. SO_4^{2-} predictions are also well correlated with observations at this site ($r = 0.8$) with moderately low bias (NMB = −16.6%). Therefore, the underpredictions of NO_3^- are not due to reduced NH_3 availability associated with SO_4^{2-} overprediction (see section 3.2 for discussion of NH_3 near Riverside). Riverside is known to experience high $PM_{2.5}$ NO_3^- concentrations when aged urban NO_x emissions mix with fresh NH_3 emissions from dairy facilities in the area [*Nowak et al.*, 2012]. The elevated NO_3^- concentrations predicted east of the LA urban core (Figure 2) are

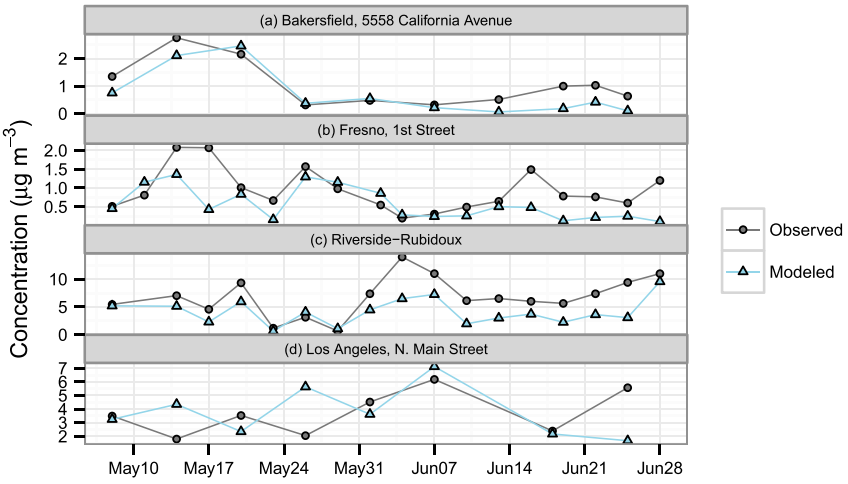

Figure 1. Comparison of 24 h average modeled and observed $PM_{2.5}$ NO_3^- concentrations at CSN monitors in SJV and SoCAB: (a) Baker-5558Ca, (b) Fresno-1st, (c) Rvrside-Rubi, and (d) Ls_Ang-NMain.

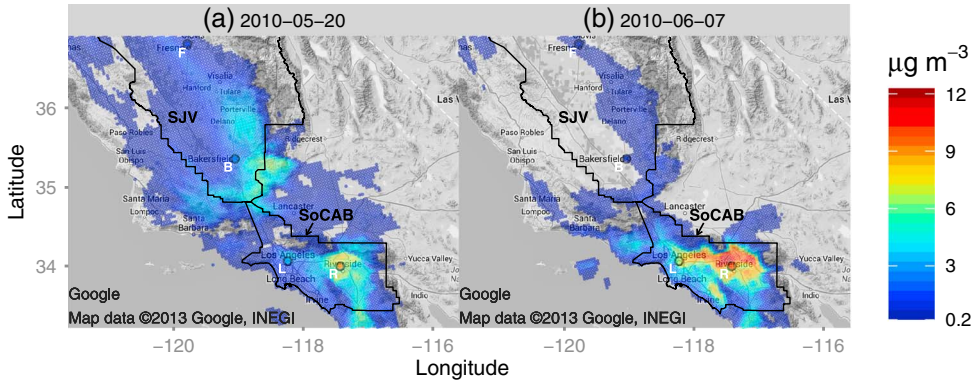

Figure 2. Model predictions of 24 h average $PM_{2.5}$ NO_3^- concentration (> 0.2 μg m^{-3}) with overlay of CSN observations on two elevated concentration days: (a) 20 May and (b) 7 June. L = Ls_Ang-NMain, R = Rvrside-Rubi, B = Baker-5558Ca, F = Fresno-1st.

consistent with this conceptual picture and the gradient in observations between the LA (Ls_Ang-NMain) and Rvrside-Rubi sites. On 7 June, the peak modeled NO_3^- concentration of 11.88 μg m^{-3} occurs just north of the Rvrside-Rubi site in Fontana (Figure 2b) and is closer to the observed value at the site (11 μg m^{-3}) than is the modeled value in the Rvrside-Rubi grid cell (7.25 μg m^{-3}).

The mean of the NO_3^- observations at the Ls_Ang-NMain monitor between 8 May and 25 June is 3.69 ± 1.62 μg m^{-3}. In contrast to results for Rvrside-Rubi, NO_3^- predictions at Ls_Ang-NMain are relatively unbiased (NMB = 2%) but are poorly correlated (r = 0.12) with observations. While the peak NO_3^- prediction occurs on the same day as the peak observation (7 June) and agrees within 13% of the observation on that day, NO_3^- is significantly overpredicted on 26 May (Figure 1d). SO_4^{2-} is also overpredicted at Ls_Ang-NMain on this day (Figure S3) indicating that the NO_3^- overprediction is not due to an excess availability of NH_3 associated with SO_4^{2-} underprediction. Modeled NO_3^- was elevated over much of SoCAB between 24 May and 27 May (Figure S6), and this time period is discussed further below in the context of the Pasadena CalNex-2010 observations.

The model captured the observed spatial pattern of lower NO_3^- concentrations in SJV than SoCAB during the study period (Figure 2). At the Bakersfield CSN site (Baker-5558Ca), the mean modeled concentration was 0.72 μg m^{-3} while the observed mean was 1.02 μg m^{-3}. Modeled NO_3^- was well correlated with observations at this site (r = 0.9). The overall low bias in model predictions at Baker-5558Ca (NMB = −31.6%) is driven largely by days after 13 June when observations were less than about 1 μg m^{-3}, and model predictions were less than about 0.5 μg m^{-3} (Figure 1a). NO_3^- predictions were also biased low at the Fresno-1st site (NMB = −39.3%). Greater underprediction of the peak observed concentrations occurred in mid-May at Fresno-1st than at Baker-5558Ca. Differences in behavior at these sites could be due in part to the greater inflow in northern SJV of marine air, which enters the Central Valley through the Carquinez straight but typically does not reach Bakersfield in the south [e.g., *Baker et al.*, 2013].

At the CSN sites, NH_4^+ predictions and observations are strongly correlated with $2SO_4^{2-} + NO_3^-$ (2SN) on a molar basis (i.e., $r \geq 0.92$; Table S4 and Figure S7) indicating that ISORROPIA II correctly captured the influence of acid condensation on NH_4^+ formation. Also, predicted and observed NH_4^+ molar concentrations were less than 2SN concentrations at all sites suggesting the possible influence of crustal cations and/or sodium on nitrate partitioning. The normalized mean difference (NMD) between NH_4^+ and 2SN was comparable for predictions and observations at Fresno-1st, Rvrside-Rubi, and Baker-5558Ca but was higher (i.e., NH_4^+ was too high relative to 2SN) for predictions (NMD = −13.7%) compared with observations (NMD = −26.9%) at Ls_Ang-NMain (Table S4). The excess modeled NH_4^+ could be related to underpredictions of Na^+ that appear to impact gas-particle partitioning near LA (see section 3.4).

3.2. Evaluation Using NOAA WP-3 Aircraft Observations

Measurements of NH_3 and HNO_3 on the NOAA WP-3 aircraft provide snapshots of mixing ratios across SoCAB and SJV that are valuable for evaluating the spatial patterns of predictions of these NH_4^+ and NO_3^- precursors. Modeled and observed mixing ratios of NH_3 along the 8 and 19 May flights are shown in Figure 3 for a

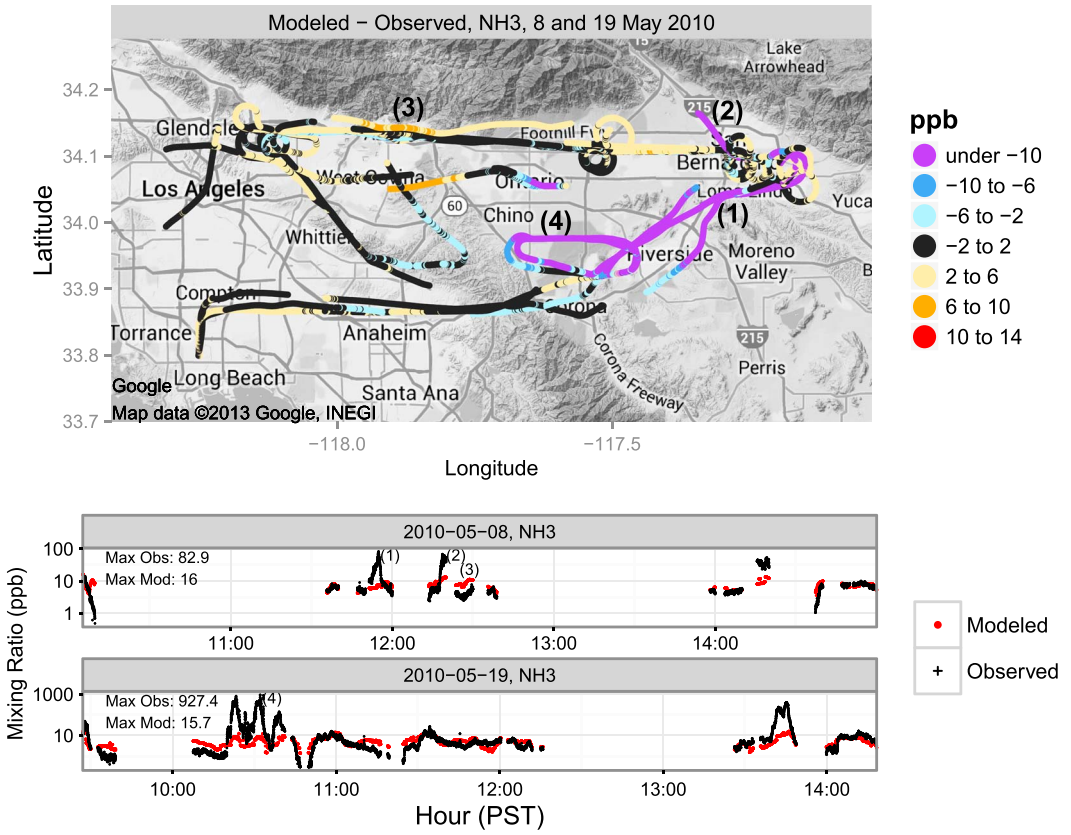

Figure 3. Observed and predicted NH_3 mixing ratios along select portions of NOAA WP-3 SoCAB flight segments and < 1500 m agl on 8 and 19 May 2010. (top) Modeled minus observed mixing ratio; (bottom) time series for predicted and observed mixing ratio on log scale. Numbers indicate locations downwind (1, 2, and 4) and upwind (3) of dairy facilities.

select region of SoCAB and < 1500 m above ground level (agl). These daytime flights sampled air masses upwind and downwind of SoCAB dairy facilities and have been discussed in earlier studies [*Neuman et al.*, 2012; *Nowak et al.*, 2012]. The altitude range was selected to focus on air masses recently impacted by surface emissions and to minimize overplotting in the figures due to overlapping flight paths in the vertical. The spatial patterns of mixing ratio differences (Figure 3 (top)) demonstrate large underpredictions of NH_3 to the east of Chino in the vicinity of Riverside (e.g., markers "(1)" and "(4)"), whereas overprediction tends to occur to the west of Chino and just south of the San Gabriel Mountains (e.g., marker "(3)"). The much higher observed peak NH_3 mixing ratios on 19 May than 8 May are due to direct sampling of dairy facility plumes during aircraft approaches to the Chino airport on 19 May.

Nowak et al. [2012] estimated NH_3 emissions from dairy facilities near Chino and from automobiles in the LA urban core based on downwind aircraft measurements. Their estimates indicate that automobile and dairy emissions may be of similar magnitude in the basin, but the dairy facility emissions have more temporal variability and are more concentrated spatially. Daily average NH_3 emission totals based on the hourly average for 12–15 PST during 7 May to 30 June are compared with the *Nowak et al.* [2012] estimates in Table 2. These hours were selected to approximate the timing of the aircraft transects used in generating the *Nowak et al.* [2012] estimates. Modeled NH_3 emissions from the agricultural sector in the relevant region of the eastern basin (28 t/d) are just below the lower end of the range estimated for dairy facilities by *Nowak et al.* [2012] (33–176 t/d). The modeled peak NH_3 mixing ratio is a factor of 4 closer to the observed peak for the 16 May transect used by *Nowak et al.* [2012] in calculating the low-end emissions estimate than for the 14 May transect used in calculating the high-end estimate (Figure S8). Accurate characterization of the large magnitude and variability of NH_3 emissions from dairy facilities present challenges for photochemical grid modeling of NH_4^+ and NO_3^- in eastern SoCAB. However, the NEI08 emissions used here for dairy facilities provide a much better representation of NH_3 emissions in SoCAB than do the NEI05 [*Schifer et al.*, 2014],

Table 2. Average NH_3 Emissions (Metric Tons per Day)

Sector	East[a]	West[a]
All[b]	35.18	43.01
Agriculture (includes dairy facilities)[b]	28.05	1.07
Mobile[b]	0.44	10.19
Area[b]	4.32	29.98
Point[b]	2.36	1.76
Nowak et al. [2012] automobiles	NA	62 ± 24
Nowak et al. [2012] dairy facilities	33 to 176	NA

[a]Regions of SoCAB defined by *Nowak et al.* [2012].
[b]Based on hours 12–15 PST for 7 May to 30 June of modeled NEI08 inventory used here.

and model bias for NO_3^- predictions in Riverside is much smaller when using NEI08 than NEI05 emissions (not shown).

Emissions from automobiles in a western region of SoCAB were estimated to be 62 ± 24 t/d by *Nowak et al.* [2012]. Although modeled NH_3 emissions from all sectors combined (43 t/d) are within the uncertainty of this estimate, modeled mobile emissions of NH_3 are only 10.2 t/d in this region suggesting that mobile emissions of NH_3 may be too low in the model. The area-source sector is the largest NH_3 emission sector in this region of the western SoCAB, and the largest categories within this sector are related to waste disposal.

In Figure 4, observed and predicted mixing ratios of HNO_3 are compared for the 8 May and 19 May flight paths just discussed for NH_3. In contrast to results for NH_3, mixing ratios of HNO_3 are overpredicted to the east of Chino and underpredicted to its west and just south of the San Gabriel Mountains. Model bias for HNO_3 predictions along these flight segments exhibits a negative correlation with that for NH_3. When the magnitude of the difference between modeled and observed HNO_3 mixing ratio is greater than 2 ppb, there is negative correlation ($r = -0.63$) between differences in modeled and observed mixing ratios for HNO_3 and NH_3. While HNO_3 mixing ratios are impacted by factors including emissions, gas-phase chemistry, and meteorology, the negative correlation in errors for NH_3 and HNO_3 predictions suggests that overpredictions of HNO_3 may be caused in part by insufficient NH_3 in the model for forming NH_4^+ and NO_3^-. The underprediction of NO_3^- in Riverside in early June discussed above could also be due in part to insufficient availability of NH_3.

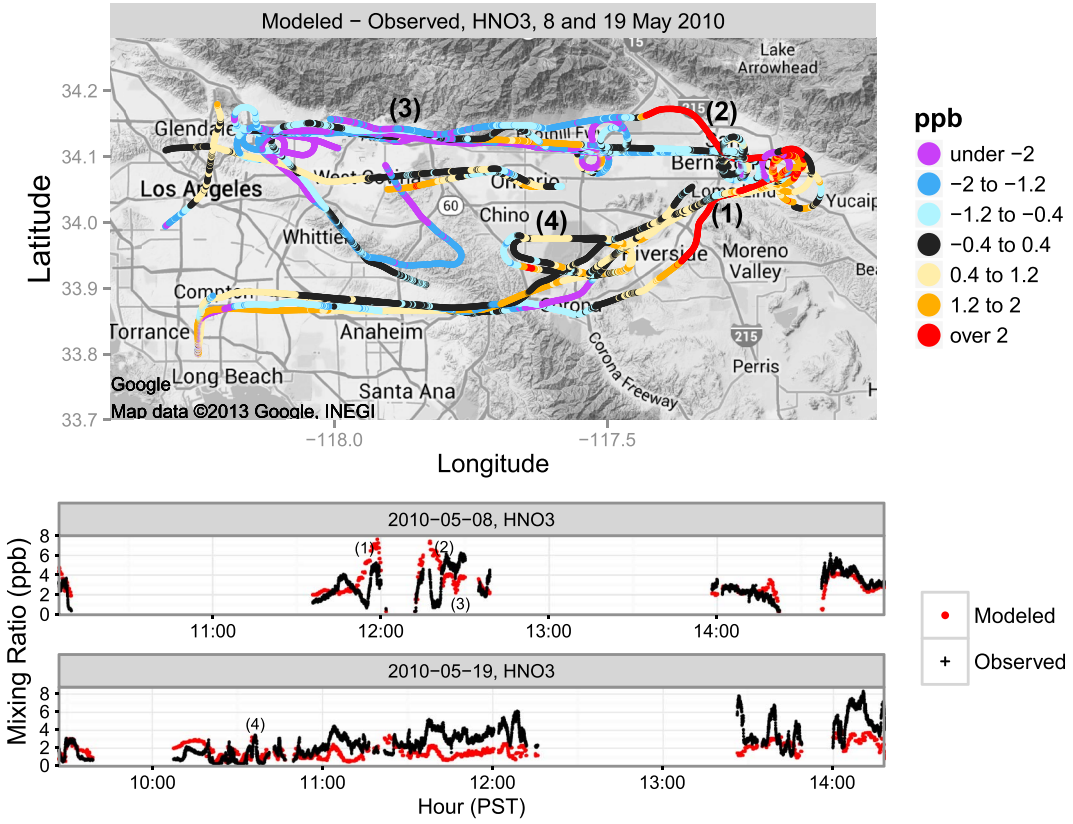

Figure 4. Same as Figure 3 but for HNO_3.

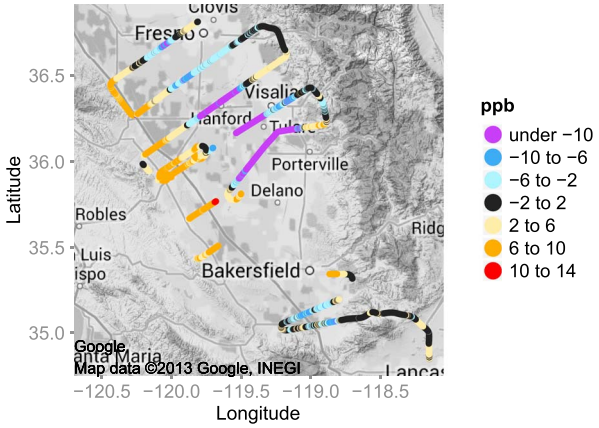

Figure 5. NH_3 mixing ratio difference (modeled − observed) along select portions of SJV flight segments < 1500 agl on 16 June 2010. See Figure S10 for mixing ratios.

Differences between modeled and observed NH_3 mixing ratios for the southern SJV flight on 16 June are shown in Figure 5. The model greatly underpredicts NH_3 mixing ratios in areas near Hanford and Tulare with large agriculture and livestock NH_3 sources. However, in western SJV and southeast of Bakersfield, the model overpredicts NH_3 for this flight. This pattern could suggest a need for improved spatial allocation of NH_3 emissions in SJV. Higher NH_3 mixing ratios were observed along the southern SJV flight on 7 May than on 16 June. The 98th percentile of observed mixing ratios was 186 ppb for the 7 May flight, compared with 41 ppb for the 16 June flight (Figures S9 and S10). Model predictions are much less variable than the observations, and the modeled 98th percentile is 19 ppb for the 7 May flight and 17 ppb for the 16 June flight. Similar to the behavior in SoCAB, HNO_3 tends to be overpredicted in highly concentrated NH_3 plumes in SJV where NH_3 is underpredicted. However, the model also tends to overpredict HNO_3 near Bakersfield where NH_3 predictions are relatively unbiased compared with aircraft observations (Figures S11 and S12).

A qualitative comparison of the spatial patterns of peak mixing ratios observed over all flights and the spatial patterns of peak modeled emissions rates was also done (not shown). In SJV, NH_3 emissions are distributed relatively evenly in the region where distinct peaks and sharp gradients in mixing ratios were observed. By contrast, in SoCAB, modeled emissions are highly concentrated near the large dairy facilities in the eastern basin where peak concentrations were observed. This qualitative comparison suggests that both the spatial allocation and magnitude of emissions require improvement in SJV, whereas the magnitude of emissions deserves more attention in SoCAB. Note also that the maximum modeled mixing ratios in the surface layer were less than about 21 ppb over all hours and grid cells in SJV and SoCAB on the flight days discussed above. Since this value is much less than the observed mixing ratios near major sources, the underpredictions of NH_3 cannot be explained in terms of a slight mismatch in time or space of the modeled plume compared with the observed plume.

3.3. Evaluation Using CalNex-2010 Ground Site Data

Comprehensive data from the Pasadena and Bakersfield ground sites enable a thorough evaluation of model performance for NH_4^+, NO_3^-, and precursors at key locations in SoCAB and SJV. The ground site data complement the 24 h average $PM_{2.5}$ measurements at the CSN sites (section 3.1) and the short spatial snapshots of NH_3 and HNO_3 from the aircraft (section 3.2).

3.3.1. Pasadena

The time series of observed and predicted HNO_3, NO_3^-, total nitrate (TN) (i.e., $HNO_3 + NO_3^-$), and the molar gas-phase fraction of TN (GFN) (i.e., $HNO_3/(HNO_3 + NO_3^-)$) at the CalNex-2010 Pasadena ground site is shown in Figure 6. In section 3.1, overprediction of NO_3^- at the LA CSN site on 26 May and underprediction at the Riverside site in early June was identified. These time periods are shaded grey in Figure 6, and data from the Pasadena site are used here to investigate causes of the errors.

In the May period, daytime PBL height, *T*, and RH are generally simulated well (Figures S15–S17), although RH is overpredicted during the night and underpredicted during the day. The modeled PBL height also appears to underrepresent the degree of mixing during the evening transition from unstable daytime to stable nighttime conditions on 24 and 25 May. The underestimate of mixing in the model in the evening on 24 May seems to cause overpredictions of NH_3 and NO (Figures 7a–7c). As a consequence of the overprediction of NO, titration of O_3 in the model causes underpredictions of O_3 (Figure 7d). Oxidation of NO and NO_2 by O_3 at night leads to production of N_2O_5 that is converted to HNO_3 via heterogeneous reaction with H_2O on

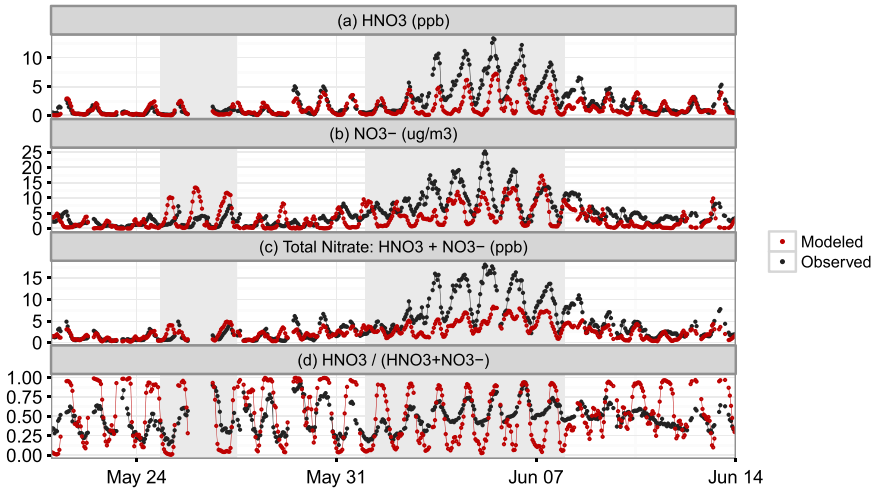

Figure 6. Comparison of measurements and predictions at Pasadena for the nitrate system. (a) HNO_3, (b) $PM_{2.5}$ NO_3^-, (c) TN: $HNO_3 + NO_3^-$, (d) GFN: HNO_3/ ($HNO_3 + NO_3^-$). Shaded regions indicate episodes discussed in section 3.3.1.

particle surfaces. Such nocturnal HNO_3 production could be overestimated for the chloride-containing particles in Pasadena (Figure S29) in publicly released versions of CMAQ, which do not include the conversion of N_2O_5 to $ClNO_2$ on particle surfaces [*Sarwar et al.*, 2012]. HNO_3 production could also be overestimated because the *Davis et al.* [2008] parameterization used in CMAQ does not account for reduced N_2O_5 reaction probabilities on particles with organic coatings [e.g., *Riemer et al.*, 2009]. The overprediction of TN associated with underestimated evening mixing and excessive oxidation of NO_x to HNO_3 translates into a large overprediction of NO_3^- because TN is predicted to partition almost entirely to the particle phase overnight, whereas observed partitioning is more moderate (Figure 6d). This overall behavior seems to explain the differences in timing of peak NO_3^- concentration for the model and observations on 24–25 May and other days (Figure 6b). However, the ceilometer measurements used here have difficulty detecting the PBL height during the transition from highly convective daytime conditions to stable nighttime conditions [*Haman et al.*, 2012]. Such limitations are evident in Figure7a, where the observed values drop to about 500 m at 18 PST but then increase to over 1000 m for most of 19–21 PST. This oscillation seems unrealistic.

In contrast to the overpredictions during 24–26 May, NO_3^- is underpredicted in Pasadena during the first week in June. *Ryerson et al.* [2013] describe how synoptic meteorology led to warm temperatures, subsiding air, and a prolonged O_3 episode in SoCAB during this period. Underpredictions of TN and O_3 during this

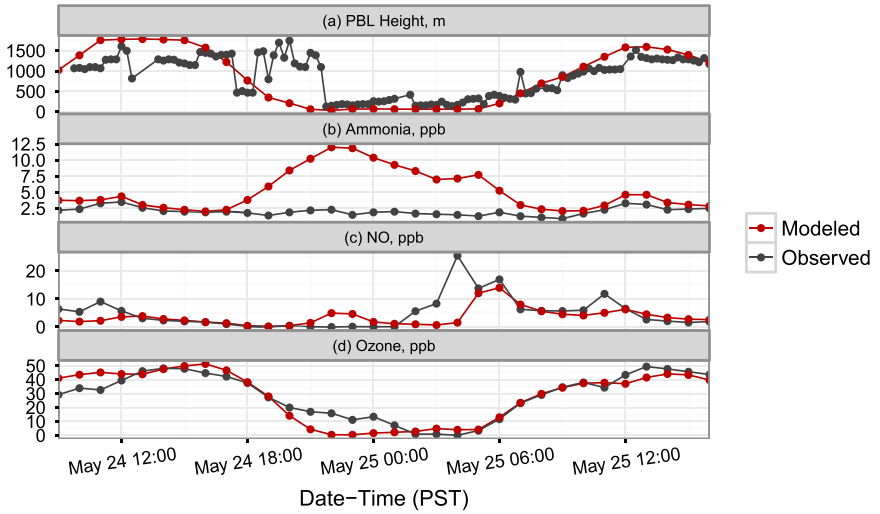

Figure 7. Time series of modeled and observed (a) PBL height and mixing ratio of (b) NH_3, (c) NO, and (d) O_3 on 24–25 May.

period suggest that the model did not capture the impact that meteorology had on air quality by enhancing multiday pollution carryover and photochemical oxidation. During 1–7 June, the daytime (11–17 PST) average NO_x-to-NO_y ratio was 0.51 for the observations (compared with 0.59 at other times), while it was 0.73 for model predictions (and 0.73 at other times). The underestimate of NO_x oxidation in the model could be due in part to oxidant limitations associated with NO_x overpredictions (Table S8).

The model did capture the relatively low PBL heights during 1–7 June (Figure S17). However, underprediction of mixing during the evening PBL transition appears to occur on some days, and daytime peaks appear to be slightly overpredicted, possibly due to differences in PBL height definitions between the model and observations. RH and *T* predictions also agree well with observed values during this period. However, wind speeds were overpredicted with a NMB of 246% for 1–7 June compared with a NMB of 208% at other times (Figure S24). The average observed wind speed at the Millikan Library in Pasadena was only 0.61 m s^{-1} during 1–7 June, but it was higher at National Weather Service sites in downtown LA (KCQT; 1.84 m s^{-1}), Riverside (KRAL; 3.17 m s^{-1}), and near the coast (KLAX, KTOA, and KSMO; 3.45 m s^{-1}). Wind speeds were overpredicted at the downtown LA site (NMB = 55%) but were underpredicted at the Riverside (NMB = −11%) and coastal sites (NMB = −24%) over the 7 May to 30 June period.

A statistical evaluation of model predictions for species just discussed as well as for additional inorganic gas and $PM_{2.5}$ components is provided in the supporting information (Table S8). NH_3 mixing ratios are overpredicted at Pasadena (NMB = 137%), and NH_4^+ concentrations are generally underpredicted (NMB = −45%) during the brief period when measurements are available (Figure S27). Also, Na^+, Cl^-, and HCl are underpredicted (NMB ≤ −76%) and poorly correlated with observations ($R \leq 0.36$) suggesting that the sea-salt emissions parameterization did not adequately represent the emissions flux, the modeled wind speeds used to drive emissions were too low, or that sea spray particles dry deposited too quickly in the model [*Kelly et al.*, 2010].

3.3.2. Bakersfield

The model was also evaluated against measurements at the Bakersfield CalNex-2010 site, where meteorology was warmer and drier with higher wind speeds than at Pasadena (Figures S14 and S37). Diurnal box plots of observed and predicted concentrations of HNO_3, NO_3^-, TN, and GFN at Bakersfield are shown in Figure 8. Similar plots for the ammonia system are shown in Figure S34. The model correctly predicted that HNO_3 and TN mixing ratios peak at about 11 PST, but daytime mixing ratios are substantially overpredicted leading to a NMB of 205% for HNO_3 (Figure 8a and Table S10). While NO_x and NO_y tend to be overpredicted at the Bakersfield site, the daytime ratio of NO_x to NO_y is greater for predictions (74%) than observations (69%). Therefore, the overpredictions of TN appear to be related to overpredictions of NO_y (a moderately conserved tracer for NO_x emissions) rather than excessive oxidation of NO_x. Such NO_y overpredictions could be related to underpredictions of PBL height; however, daytime PBL heights appear to be simulated well in SJV during this period [*Baker et al.*, 2013] suggesting that an overestimate of NO_x emissions could be the primary cause. While HNO_3 is overpredicted at all hours of the day, NO_3^- is typically underpredicted except at hours 5–6 PST when TN partitions more readily to the particle phase (Figures 8b and 8d).

Modeled NH_4^+ has a diurnal pattern similar to NO_3^- and was underpredicted at all hours except for roughly 5–7 PST (Figure S34). NH_4^+ was strongly correlated with 2SN in both measurements ($r = 0.84$) and predictions ($r = 0.91$) and was generally less than 2SN for the observations (NMD = −18.1%) and predictions (NMD = −29%). Differences in the relationship between NH_4^+ and 2SN for the model and observations could be related to different impacts of crustal cations on particle acidity. NH_3 mixing ratios are underpredicted at Bakersfield for most hours except for those during and just after the modeled evening PBL transition (18–22 PST) when they are overpredicted. Too early stabilization of the modeled PBL could be the reason for this overprediction rather than the temporal allocation of NH_3 emissions, since NO_x is also overpredicted at this time, ozone is titrated, and NH_3 emissions from the agricultural sector peak earlier in the day (~14 PST) (Figures S35 and S36).

3.4. Gas-Particle Partitioning

Differences in observed and predicted partitioning of TN between the gas and particle phases at the CalNex-2010 ground sites are evident in Figures 6d and 8d. Here we conduct 0-D ISORROPIA II simulations to explore possible causes of these differences. ISORROPIA II accounts for the impact of crustal cations and has been used successfully to interpret observations previously [*Fountoukis et al.*, 2009; *Zhang et al.*, 2002].

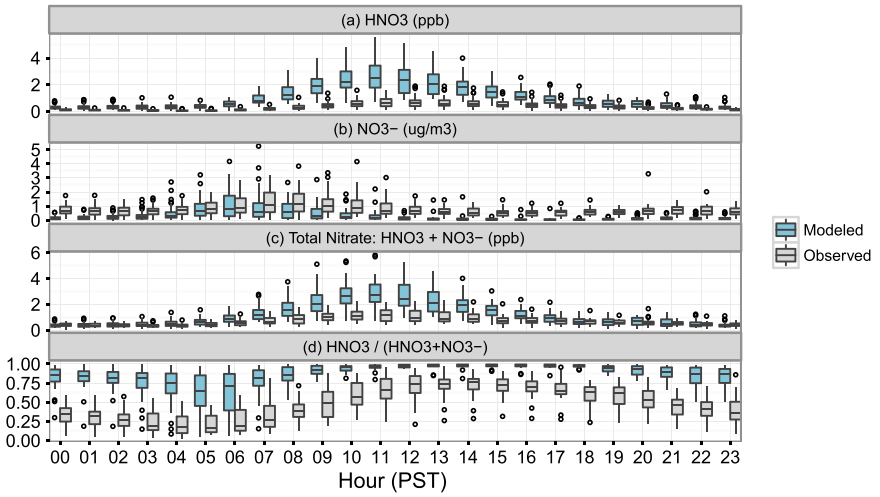

Figure 8. Comparison of diurnal distributions of measurements and predictions at the CalNex-2010 Bakersfield site for the nitrate system during 22 May to 28 June. (a) HNO_3, (b) $PM_{2.5}$ NO_3^-, (c) TN: $HNO_3 + NO_3^-$, (d) GFN: $HNO_3/(HNO_3 + NO_3^-)$. Circles indicate data more than 1.5 times the interquartile range from either end of the box.

The metastable branch of ISORROPIA II, where salts do not crystallize and supersaturated solutions exist for RHs below the mutual deliquescence RH, is used in all calculations unless otherwise noted. This branch was selected based on the RH observations in Pasadena and because it is the approach used in the CMAQ model under investigation. Note that the phase states of inorganic salts in ambient particles are often uncertain due to deviations from laboratory measurements of deliquescence for bulk solutions [*Robinson and Stokes*, 1970] and efflorescence for levitated droplets [e.g., *Chan et al.*, 1992]. In any event, gas-particle partitioning calculations for NH_4^+ and NO_3^- are often insensitive to phase state (e.g., see *Langridge et al.* [2012], and the Bakersfield discussion below).

At the Pasadena site, the model partitions too much of TN to the particle phase at night and too much to the gas phase during the day (Figure 6d). Some of the disagreement between predictions and observations in the early morning (3–6 PST) is due to the sensitivity of the chemical ionization mass spectrometry (CIMS) measurement to particle nitrate, wherein some NO_3^- volatilizes in the inlet and is measured as gas-phase HNO_3. In Figure 9, GFN predictions of ISORROPIA II are shown as a function of TA (i.e., $NH_3 + NH_4^+$), and TN based on simulations where values of *T*, RH, SO_4^{2-}, Na^+, K^+, Ca^{2+}, Mg^{2+}, and total chloride (i.e., $HCl + Cl^-$) are fixed at the average values of the model predictions (Figure 9 (left)) or observations (Figure 9 (right)) for two time periods: 14–16 PST (Figure 9 (top)) and 0–3 PST (Figure 9 (bottom)). Since Ca^{2+} and Mg^{2+} were not measured, predicted values were used for these ions in calculations for the "observed-conditions" cases. The markers in Figure 9 correspond to modeled (open circles) and observed (squares) mixing ratios of TA and TN at matching hours.

For daytime conditions (Figure 9 (top)), GFN predictions of ISORROPIA II for "modeled conditions" (Figure 9 (left)) indicate a broader region of high partitioning to the gas phase than those for observed conditions (Figure 9 (right)) (see below for explanation). This pattern is consistent with the daytime overprediction of GFN in Figure 6d. Notice that the markers for model predictions overlap a region of high GFN (red region) for the modeled-conditions case but overlap a region of moderate GFN (orange region) for the observed-conditions case. For hours where measurements are available, predictions tend to underestimate the observed TN during the day; however, errors in TN and TA have a smaller impact on GFN than do errors in other aspects of the system during daytime hours.

For the nighttime period (Figure 9 (bottom)), the gradients in GFN as a function of TA and TN are similar for conditions based on modeled (Figure 9 (left)) and observed (Figure 9 (right)) values. However, TA mixing ratios are overpredicted, and the markers for predictions overlap a region of lower GFN than the region overlapped by markers for observations. The primary cause of underpredictions of GFN during the nighttime hours therefore appears to be overprediction of TA. These overpredictions could be caused in part by the apparent underpredictions of mixing in nighttime PBL (e.g., Figure 7a).

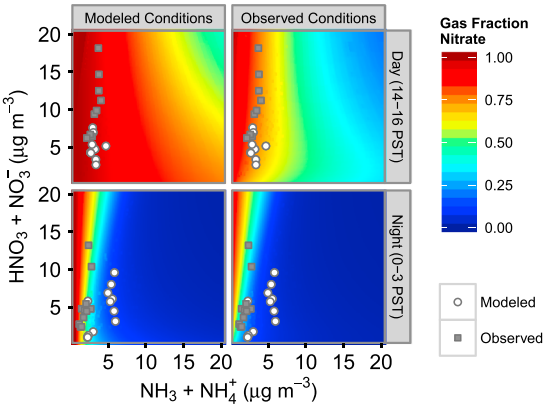

Figure 9. ISORROPIA II predictions of molar gas fraction of nitrate, $HNO_3/(HNO_3 + NO_3^-)$, as a function of TA and TN based on average (left) modeled and (right) observed conditions at Pasadena for *T*, RH, SO_4^{2-}, TCL, Na^+, Ca^{2+}, K^+, and Mg^{2+} during (top) 14–16 PST and (bottom) 0–3 PST. Markers correspond to observed and predicted TA and TN concentrations at matching hours. Note: Ca^{2+} and Mg^{2+} were not measured, and so modeled values were used for these ions in observed-conditions cases.

To identify which differences in modeled and observed conditions caused the differences in GFN predictions for daytime conditions (Figure 9 (top)), we conducted additional ISORROPIA II sensitivity simulations where select values in the modeled-conditions case were set to the values in the observed-conditions case. In Figure 10, ISORROPIA II predictions of GFN for the daytime observed-conditions case are compared with those for the base modeled-conditions case and the sensitivity modeled-conditions scenarios at observed and modeled levels of TA and TN. GFN predictions of ISORROPIA II are greater than 0.5 under both modeled and observed conditions, but predictions for the base modeled-conditions case are much higher than those under observed conditions (NMB = 31%). When the Na^+ concentration for the daytime modeled-conditions case (4 nmol m^{-3}) is increased to match the observed value (40 nmol m^{-3}), more of TN partitions to the particle phase and better agreement occurs (Figure 10, blue markers; NMB = 10%). This behavior is consistent with the nature of Na^+ as a nonvolatile cation. Differences in average RH during daytime for the model (RH = 43%) and observations (RH = 53%) also impact GFN, and good agreement between ISORROPIA II predictions occurs when RH and Na^+ values in the modeled-conditions case are set to observed values (Figure 10, orange markers; NMB = 2.5%). The sensitivity run with increased Na^+ concentration also yielded lower NH_4^+ concentration, and this behavior is consistent with the overprediction of NH_4^+ relative to 2SN noted in section 3.1 for the LA CSN site. Therefore, improving predictions of Na^+ should improve predictions of gas-particle partitioning for both TN and TA. Na^+ predictions could be improved by tailoring the model representation of the coastal surf zone as well as the size distribution and magnitude of the sea spray emissions flux to conditions along the SoCAB coast.

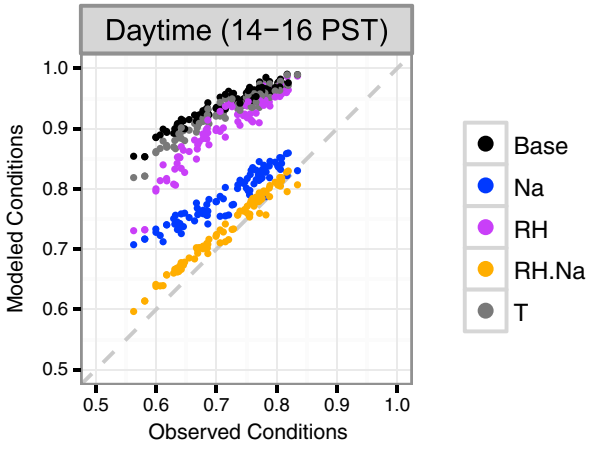

Figure 10. ISORROPIA II predictions of molar GFN at observed and predicted TA and TN levels based on average observed and modeled conditions during 14–16 PST as in Figure 9. Markers correspond to the base modeled-conditions case and sensitivity cases where select values for the modeled-conditions case (i.e., Na^+, RH, RH and Na^+, and *T*) were set to observed values.

Similar analysis was conducted to understand gas-particle partitioning at the Bakersfield site, where GFN was overpredicted at all hours (Figure 8d). For nighttime hours (0–3 PST), the lower average RH for the model (RH = 44%) than the measurements (RH = 52%) contributed to the overprediction of GFN (Figure S45). Underpredictions of TA at some hours also appear to contribute to the GFN overpredictions at night (Figure S46 (bottom)). For daytime hours in Bakersfield, the RH was low (e.g., mean observed RH = 22%), and the particle ionic strength exceeded the cap of 100 *m* in ISORROPIA II (Figure S47). Although predictions of GFN for the metastable branch of ISORROPIA II are likely compromised under such

conditions, they are in general agreement with those of the stable branch of ISORROPIA II for observed and modeled TA and TN levels (Figures S46 and S48 (top)).

Errors in predictions of gas-particle partitioning of TN in Bakersfield could also be due to errors in predictions of crustal cations and the lack of treatment of the effects of organic acids and amines on inorganic aerosol thermodynamics. For instance, overpredictions of GFN (and HNO_3) might be explained by underpredictions of carbonate-containing dust, since carbonates can enhance condensation of gas-phase acids including HNO_3 [e.g., *Kelly and Wexler*, 2005]. However, the presence of additional carbonates could worsen overpredictions of the gas fraction of TA at some hours by causing more of the total NH_x to exist in the gas phase. Note that dust concentrations are likely to be relatively low and RH conditions high enough to be well represented by the metastable branch of ISORROPIA II during humid and stagnant wintertime $PM_{2.5}$ episodes in SJV.

4. Conclusions

The fine-scale CMAQ simulation captured the basic features of NH_4^+ and NO_3^- formation in SoCAB and SJV. For instance, NO_3^- predictions were well correlated with CSN observations in Bakersfield and Riverside, and elevated NO_3^- concentrations were predicted downwind of the dairy facilities in eastern SoCAB. However, the examination of differences in model predictions and measurements indicates areas where increased understanding will improve model performance. First, inventoried NH_3 emissions from dairy and livestock facilities in SoCAB and SJV appear to be too low and do not capture the apparently large variability in emissions from these facilities. Additionally, the spatial allocation of NH_3 emissions in SJV may require development. Underpredictions of NO_3^- concentration in Riverside may be caused in part by NH_3 emission deficits. Conversely, NH_3 emissions may be too high near Pasadena, as NH_3 mixing ratios were overpredicted there. Considering that NH_3 emissions from automobiles in the LA area appear to be too low, the overpredictions of NH_3 mixing ratios in Pasadena suggest that emissions related to other major sources in this region (i.e., waste disposal-related area sources) could be overestimated. Offline ISORROPIA II simulations suggest that overpredictions of TA at Pasadena can cause too much partitioning of TN to the particle phase at night, while underpredictions of Na^+ can cause too much partitioning of TN to the gas phase during the day. Also, underpredictions of Cl^- could impact HNO_3 production via heterogeneous N_2O_5 reactions at night. Therefore, sea spray emissions parameterizations should be revisited for the SoCAB coast, although underpredictions of wind speed over water and too rapid particle deposition could also contribute to sea salt-related prediction errors. Underpredictions of mixing during the evening PBL transition appears to concentrate pollutant precursors and lead to excess nitrate formation via the N_2O_5 pathway on some nights in Pasadena. This behavior highlights a need for better representations in WRF of urban heat island effects or other features that influence the evening PBL transition. Overall, the analyses demonstrate variations in model performance within and across the air basins and suggest that improvements in areas of emissions, meteorology, and chemistry modeling could improve fine-scale simulations for these highly populated NAAQS nonattainment areas.

Acknowledgments
Discussions with Prakash Bhave, Rohit Mathur, and Jon Pleim of U.S. EPA (ORD) contributed to this work. The authors thank Allen H. Goldstein, Robert J. Weber, and Ronald C. Cohen of UC Berkeley for providing meteorology, O_3, and organic nitrate data at Bakersfield. We also thank Barry Lefer of the University of Houston for providing ceilometer and NO_x data at Pasadena and Paul O. Wennberg of Cal Tech for providing HNO_3 data at Bakersfield. The authors also recognize the contributions of Chris Allen, Allan Beidler, James Beidler, Alison Eyth, Rich Mason, Norm Possiel, Alexis Zubrow, and Tyler Fox, and we thank the three anonymous reviewers for helpful suggestion.

References

Angevine, W. M., L. Eddington, K. Durkee, C. Fairall, L. Bianco, and J. Brioude (2012), Meteorological model evaluation for CalNex 2010, *Mon. Weather Rev.*, *140*(12), 3885–3906, doi:10.1175/MWR-D-12-00042.1.

Baker, K. R., C. Misenis, M. D. Obland, R. A. Ferrare, A. Scarino, and J. T. Kelly (2013), Evaluation of surface and upper air fine scale WRF meteorological modeling of the May and June 2010 CalNex period in California, *Atmos. Environ.*, *8*, 299–309.

Bishop, G. A., A. M. Peddle, D. H. Stedman, and T. Zhan (2010), On-road emission measurements of reactive nitrogen compounds from three California cities, *Environ. Sci. Technol.*, *44*(9), 3616–3620, doi:10.1021/es903722p.

Bishop, G. A., B. G. Schuchmann, and D. H. Stedman (2012), Emission changes resulting from the San Pedro Bay, California ports truck retirement program, *Environ. Sci. Technol.*, *46*(1), 551–558, doi:10.1021/es202392g.

California Department of Food and Agriculture (2013), California agricultural statistics review 2012–2013, California Department of Food and Agriculture. [Available at http://www.cdfa.ca.gov/statistics/.]

California Department of Finance (2013), Projections of population and births. [Available at http://www.dof.ca.gov/research/demographic/reports/projections/.]

Chan, C. K., R. C. Flagan, and J. H. Seinfeld (1992), Water activities of $NH_4NO_3/(NH_4)_2SO_4$ solutions, *Atmos. Environ.*, *26A*(9), 1661–1673.

Crounse, J. D., K. A. McKinney, A. J. Kwan, and P. O. Wennberg (2006), Measurement of gas-phase hydroperoxides by chemical ionization mass spectrometry, *Anal. Chem.*, *78*, 6726–6732.

Davis, J. M., P. V. Bhave, and K. M. Foley (2008), Parameterization of N2O5 reaction probabilities on the surface of particles containing ammonium, sulfate, and nitrate, *Atmos. Chem. Phys.*, *8*, 5295–5311.

Ellis, R. A., J. G. Murphy, E. Pattey, R. van Haarlem, J. M. O'Brien, and S. C. Herndon (2010), Characterizing a quantum cascade tunable infrared laser differential absorption spectrometer (QC-TILDAS) for measurements of atmospheric ammonia, *Atmos. Meas. Tech.*, *3*, 397–406.

Ensberg, J. J., et al. (2013), Inorganic and black carbon aerosols in the Los Angeles Basin during CalNex, *J. Geophys. Res. Atmos.*, *118*, 1777–1803, doi:10.1029/2012JD018136.

Fast, J. D., et al. (2012), Transport and mixing patterns over Central California during the carbonaceous aerosol and radiative effects study (CARES), *Atmos. Chem. Phys.*, *12*, 1759–1783, doi:10.5194/acp-12-1759-2012.

Fountoukis, C., and A. Nenes (2007), ISORROPIA II: A computationally efficient thermodynamic equilibrium model for K^+-Ca^{2+}-Mg^{2+}-NH_4^+-Na^+-SO_4^{2-}-NO_3^--Cl^-–H_2O aerosol, *Atmos. Chem. Phys.*, *7*(17), 4639–4659.

Fountoukis, C., A. Nenes, A. Sullivan, R. Weber, T. Van Reken, M. Fischer, E. Matías, M. Moya, D. Farmer, and R. C. Cohen (2009), Thermodynamic characterization of Mexico City aerosol during MILAGRO 2006, *Atmos. Chem. Phys.*, *9*, 2141–2156, doi:10.5194/acp-9-2141-2009.

Haman, C. L., B. L. Lefer, and G. A. Morris (2012), Seasonal variability in the diurnal evolution of the boundary layer in a near coastal urban environment, *J. Atmos. Oceanic Technol.*, *29*, 697–710, doi:10.1175/JTECH-D-11-00114.1.

Heald, C. L., et al. (2012), Atmospheric ammonia and particulate inorganic nitrogen over the United States, *Atmos. Chem. Phys.*, *12*, 10,295–10,312.

Herner, J. D., Q. Ying, J. Aw, O. Gao, D. P. Y. Chang, and M. J. Kleeman (2006), Dominant mechanisms that shape the airborne particle size and composition distribution in central California, *Aerosol Sci. Technol.*, *40*(10), 827–844, doi:10.1080/02786820600728668.

Hixson, M., A. Mahmud, J. Hu, and M. J. Kleeman (2012), Resolving the interactions between population density and air pollution emissions controls in the San Joaquin Valley, USA, *J. Air Waste Manage. Assoc.*, *62*(5), 566–575, doi:10.1080/10962247.2012.663325.

Huang, M., K. W. Bowman, G. R. Carmichael, R. B. Pierce, H. M. Worden, M. Luo, O. R. Cooper, I. B. Pollack, T. B. Ryerson, and S. S. Brown (2013), Impact of Southern California anthropogenic emissions on ozone pollution in the mountain states: Model analysis and observational evidence from space, *J. Geophys. Res. Atmos.*, *118*, 12,784–12,803, doi:10.1002/2013JD020205.

Jacobson, M. Z. (2002), *Atmospheric Pollution: History, Science, and Regulation*, 412 pp., Cambridge Univ. Press, Cambridge, U. K.

Kelly, J. T., and A. S. Wexler (2005), Thermodynamics of carbonates and hydrates related to heterogeneous reactions involving mineral aerosol, *J. Geophys. Res.*, *110*, D11201, doi:10.1029/2004JD005583.

Kelly, J. T., P. V. Bhave, C. G. Nolte, U. Shankar, and K. M. Foley (2010), Simulating emission and chemical evolution of coarse sea-salt particles in the Community Multiscale Air Quality (CMAQ) model, *Geosci. Model Dev.*, *3*, 257–273, doi:10.5194/gmd-3-257-2010.

Kelly, J. T., C. Cai, J. Avise, and A. Kaduwela (2011), Simulating particle size distributions over California and impact on lung deposition fraction, *Aerosol Sci. Technol.*, *45*(2), 148–162.

Kleeman, M. J., Q. Ying, and A. Kaduwela (2005), Control strategies for the reduction of airborne particulate nitrate in California's San Joaquin Valley, *Atmos. Environ.*, *39*(29), 5325–5341, doi:10.1016/j.atmosenv.2005.05.044.

Langridge, J. M., et al. (2012), Evolution of aerosol properties impacting visibility and direct climate forcing in an ammonia-rich urban environment, *J. Geophys. Res.*, *117*, D00V11, doi:10.1029/2011JD017116.

Lu, R., and R. P. Turco (1996), Ozone distributions over the Los Angeles basin: Three-dimensional simulations with the SMOG model, *Atmos. Environ.*, *30*(24), 4155–4176, doi:10.1016/1352-2310(96)00153-7.

Markovic, M. Z., T. C. VandenBoer, and J. G. Murphy (2012), Characterization and optimization of an online system for the simultaneous measurement of atmospheric water-soluble constituents in the gas and particle phases, *J. Environ. Monit.*, *14*, 1872–1884.

Neuman, J. A., et al. (2002), Fast-response airborne in situ measurements of HNO3 during the Texas 2000 Air quality study, *J. Geophys. Res.*, *107*(D20), 4436, doi:10.1029/2001JD001437.

Neuman, J. A., et al. (2012), Observations of ozone transport from the free troposphere to the Los Angeles basin, *J. Geophys. Res.*, *117*, D00V09, doi:10.1029/2011JD016919.

Nowak, J. B., J. A. Neuman, K. Kozai, L. G. Huey, D. J. Tanner, J. S. Holloway, T. B. Ryerson, G. J. Frost, S. A. McKeen, and F. C. Fehsenfeld (2007), A chemical ionization mass spectrometry technique for airborne measurements of ammonia, *J. Geophys. Res.*, *112*, D10S02, doi:10.1029/2006JD007589.

Nowak, J. B., J. A. Neuman, R. Bahreini, A. M. Middlebrook, J. S. Holloway, S. A. McKeen, D. D. Parrish, T. B. Ryerson, and M. Trainer (2012), Ammonia sources in the California South Coast Air Basin and their impact on ammonium nitrate formation, *Geophys. Res. Lett.*, *39*, L07804, doi:10.1029/2012GL051197.

Pleim, J. E. (2007), A combined local and nonlocal closure model for the atmospheric boundary layer. Part II: Application and evaluation in a mesoscale meteorological model, *J. Appl. Meteorol. Climatol.*, *46*, 1396–1409.

Pleim, J. E., and A. J. Xiu (2003), Development of a land surface model. Part II: Data assimilation, *J. Appl. Meteorol.*, *42*, 1811–1822.

Pusede, S. E., and R. C. Cohen (2012), On the observed response of ozone to NOx and VOC reactivity reductions in San Joaquin Valley California 1995-present, *Atmos. Chem. Phys.*, *12*(18), 8323–8339, doi:10.5194/acp-12-8323-2012.

Pye, H. O. T., et al. (2013), Epoxide pathways improve model predictions of isoprene markers and reveal Key role of acidity in aerosol formation, *Environ. Sci. Technol.*, *4*, 11,056–11,064, doi:10.1021/es402106h.

Riedel, T. P., et al. (2012), Nitryl chloride and molecular chlorine in the coastal marine boundary layer, *Environ. Sci. Technol.*, *46*(19), 10,463–10,470, doi:10.1021/es204632r.

Riemer, N., H. Vogel, B. Vogel, T. Anttila, A. Kiendler-Scharr, and T. F. Mentel (2009), Relative importance of organic coatings for the heterogeneous hydrolysis of N_2O_5 during summer in Europe, *J. Geophys. Res.*, *114*, D17307, doi:10.1029/2008JD011369.

Robinson, R. A., and R. H. Stokes (1970), *Electrolyte Solutions*, Butterworth, London.

Rollins, A. W., et al. (2012), Evidence for NOx control over nighttime SOA formation, *Science*, *337*(6099), 1210–1212, doi:10.1126/science.1221520.

Russell, A. G., and G. R. Cass (1986), Verification of a mathematical model for aerosol nitrate and nitric acid formation and its use for control measure evaluation, *Atmos. Environ.*, *20*, 2011–2025, doi:10.1016/0004-6981(86)90342-2.

Ryerson, T. B., et al. (2013), The 2010 California Research at The Nexus of Air Quality and Climate Change (CalNex) field study, *J. Geophys. Res. Atmos.*, *118*, 5830–5866, doi:10.1002/jgrd.50331.

Sarwar, G., H. Simon, P. Bhave, and G. Yarwood (2012), Examining the impact of heterogeneous nitryl chloride production on air quality across the United States, *Atmos. Chem. Phys.*, *12*, 6455–6473, doi:10.5194/acp-12-6455-2012.

South Coast Air Quality Management District (2013), South coast air quality management district final 2012 air quality management plan, appendix II. [Available at http://www.aqmd.gov/aqmp/2012aqmp/Final-February2013/MainDoc.pdf.]

Schifer, L. D., C. L. Heald, J. B. Nowak, J. S. Holloway, J. A. Neuman, R. Bahreini, I. B. Pollack, T. B. Ryerson, C. Wiedinmyer, and J. G. Murphy (2014), An investigation of ammonia and inorganic particulate matter in California during the CalNex campaign, *J. Geophys. Res. Atmos.*, doi:10.1002/2013JD020765.

Simon, H., K. R. Baker, and S. Phillips (2012), Compilation and interpretation of photochemical model performance statistics published between 2006 and 2012, *Atmos. Environ.*, *61*, 124–139.

San Joaquin Valley Air Pollution Control District (2012), San Joaquin Valley air pollution control district 2012 PM2.5 plan. [Available at http://www.valleyair.org/Air_Quality_Plans/PM25Plan2012/CompletedPlanbookmarked.pdf.]

U.S. Environmental Protection Agency (U.S. EPA) (2009), Integrated science assessment for particulate matter (final report), *EPA/600/R-08/139F*, U.S. Environmental Protection Agency, Washington, D. C.

U.S. EPA (2012a), Regulatory impact analysis for the final revisions to the national ambient Air quality standards for particulate matter, *EPA-452/R-12-005*, U.S. Environmental Protection Agency, Washington, D. C.

U.S. EPA (2012b), Technical support document (TSD) preparation of emissions inventories for the version 5.0, 2007 emissions modeling platform. [Available at http://epa.gov/ttn/chief/emch/2007v5/2007v5_2020base_EmisMod_TSD_13dec2012.pdf.]

U.S. EPA (2013), PM2.5 design value report. [Available at http://www.epa.gov/airtrends/values.html, accessed 5 Sept. 2013.]

Veres, P., J. M. Roberts, C. Warneke, D. Welsh-Bon, M. Zahniser, S. Herndon, R. Fall, and J. de Gouw (2008), Development of negative-ion proton-transfer chemical-ionization mass spectrometry (NI-PT-CIMS) for the measurement of gas-phase organic acids in the atmosphere, *Int. J. Mass Spectrom.*, *274*, 48–55, doi:10.1016/j.ijms.2008.04.032.

Walker, J. M., S. Philip, R. V. Martin, and J. H. Seinfeld (2012), Simulation of nitrate, sulfate, and ammonium aerosols over the United States, *Atmos. Chem. Phys.*, *12*, 11,213–11,227.

Weber, R. J., D. Orsini, Y. Daun, Y.-N. Lee, P. J. Klotz, and F. Brechtel (2001), A particle-into-liquid collector for rapid measurements of aerosol bulk chemical composition, *Aerosol Sci. Technol.*, *35*, 718–727, doi:10.1080/02786820152546761.

Yarwood, G., S. Rao, M. Tocke, and G. Z. Whitten (2005), Updates to the carbon bond mechanism: CB05, Report to the U.S. Environmental Protection Agency, ENVIRON International Corporation, Novato. [Available at http://www.camx.com/publ/pdfs/CB05_Final_Report_120805.pdf.]

Ying, Q. (2011), Physical and chemical processes of wintertime secondary nitrate aerosol formation, *Front. Environ. Sci. Eng. China*, *5*(3), 348–361, doi:10.1007/s11783-011-0343-1.

Young, C. J., et al. (2012), Vertically resolved measurements of nighttime radical reservoirs in Los Angeles and their contribution to the urban radical budget, *Environ. Sci. Technol.*, *46*(20), 10,965–10,973, doi:10.1021/es302206a.

Zhang, J., W. Chameides, R. Weber, G. Cass, D. Orsini, E. Edgerton, P. Jongejan, and J. Slanina (2002), An evaluation of the thermodynamic equilibrium assumption for fine particulate composition. Nitrate and ammonium during the 1999 Atlanta Supersite Experiment, *J. Geophys. Res.*, *108*(D7), 8414, doi:10.1029/2001JD001592.